RESEARCH ARTICLE | MAY 16 2025

# Optical identification and anti-counterfeiting based on plasmonic core–shell nanoparticles with Fano resonance

Nga Vu ; Mohamed Farhat ; Chien-Hao Liu ; Pai-Yen Chen



*Appl. Phys. Lett.* 126, 191105 (2025)
https://doi.org/10.1063/5.0262965

Applied Physics Letters ARTICLE pubs.aip.org/aip/apl

# Optical identification and anti-counterfeiting based on plasmonic core–shell nanoparticles with Fano resonance

Cite as: Appl. Phys. Lett. **126**, 191105 (2025); doi: 10.1063/5.0262965
Submitted: 11 February 2025 · Accepted: 2 May 2025 ·
Published Online: 16 May 2025

View Online Export Citation CrossMark

Nga Vu,[1] Mohamed Farhat,[2] Chien-Hao Liu,[3] and Pai-Yen Chen[1,a)]

## AFFILIATIONS

[1]Department of Electrical and Computer Engineering, University of Illinois at Chicago, Chicago, Illinois 60607, USA
[2]Computer, Electrical, and Mathematical Sciences and Engineering Division, King Abdullah University of Science and Technology (KAUST), Thuwal 23955-6900, Saudi Arabia
[3]Department of Mechanical Engineering, National Taiwan University, Taipei 10617, Taiwan

[a)]Author to whom correspondence should be addressed: pychen@uic.edu

## ABSTRACT

Fano resonance with an asymmetric and ultrasharp resonant line shape has been extensively studied in various light scattering scenes, unlocking several applications for sensing, information processing, and optical identification. Fano resonance appearing in multilayered nanoparticles (NPs) is particularly intriguing as its sharp and comb-like resonant line shape may enable optical identification at the nanoscale. We herein propose the concept of the optical physical unclonable function (PUF) based on the scattering responses of core–shell (plasmonic-dielectric) NPs. Specifically, the sharp, asymmetric spectral responses near the Fano resonance frequency, which are highly sensitive to perturbations (e.g., nanomanufacturing imperfections), can be exploited as a unique electromagnetic fingerprint for PUF-based identification and anti-counterfeiting applications. Here, we theoretically and statistically demonstrate that scattering from Fano-resonant multilayered NPs can be regarded as a perfect entropy source for the generation of PUF encryption keys, with outstanding performance in terms of uniqueness, randomness, encoding capacity, and NIST randomness test results. The proposed optical PUF opens pathways to implement nano-tags for optical identification, authentication, and anti-counterfeiting applications.





Rapid advances in nanotechnology have enabled the engineering of optical coupling in nanoparticle (NP) assemblies, giving rise to the exotic Fano resonance,[1–3] electromagnetically induced transparency,[4,5] and bounded states in continuum (BIC)[6,7] in the realm of nanophotonics and nano-optics. In general, Fano resonance found in various wave scattering phenomena is formed by the spectral interference between a narrowband dark mode and a broadband bright mode or a continuum, with its spectral features that can be well described by Fano formula.[8] The asymmetric and ultrasharp Fano resonance, with an extraordinary high-quality factor (Q-factor), has enabled a variety of optical and photonic applications, such as optical switching,[9] filtering,[10] sensing,[11,12] and optical identification (optical ID).[13] Recently, comb-like Fano resonance has been observed in a multilayered plasmonic NP,[14,15] of which resonant scattering modes (bright mode) and invisible modes at which scattered fields are canceled (dark mode) are intertwined in the scattering cross section (SCS) spectrum.[16] The ultrasharp and comb-like resonant scattering response is of particular interest for the realization of passive optical ID, which, in some sense, is analogous to chipless radio frequency identification (RFID) tags based on an array of dipole resonators.[17,18] Francesco and Alu have designed a 3-bits optical tag using a dielectric NP coated with three plasmonic layers, of which the bit sequence is encoded in peaks of the detected SCS spectrum.[13] Unlike conventional optical ID technologies, such as optical character recognition (OCR),[19] image recognition,[20] and barcode or quick-response code (QR),[21] this nanophotonics-based ID and labeling technology is much less vulnerable to unnoticed replication and unauthorized duplication, preventing the ID from malicious hardware trojan. Compared to other nanophotonic-based security technologies, the NP-based physical unclonable function (PUF) offers a compelling balance between scalability and simplicity. While metasurfaces or holographic tags require high-resolution lithography and precise patterning,[22,23] the nanoparticle PUF solely relies

on stochastic self-assembly and intrinsic material composition randomness, which is naturally introduced during colloidal synthesis, to generate the optical fingerprint. Compared to photonic crystal or fluorescent tags, nanoparticle PUF is less sensitive to angle view readability and less fragile to be damaged.[24] Although optical ID tags based on multilayered nanoparticles (NPs) may be readily synthesized in a cost-effective manner, the bit sequence is hardly scalable because the number of binary bits encoded in the SCS spectrum is proportional to the number of plasmonic covers. Given the complexity of nanofabricating multilayered NPs including more than two layers, it may be impractical for optical ID tags to store more than 4 bits,[13] thus posing a challenge to the encoding capacity.

In this work, we introduce a robust and scalable optical ID tag made of a two-layer core–shell (plasmonic-dielectric) NP, which can be readily and massively manufactured. Specifically, the optical ID is based on the physical unclonable function (PUF) derived from the spectral scattering characteristics near the Fano resonance, as illustrated in Fig. 1. In the practical synthesis of core–shell NPs, especially during the large-scale or batch-scale-up fabrication, manufacturing imperfections generally arise due to challenges in maintaining uniform chemical reaction conditions.[25,26] In particular, variations in reagent mixing, temperature distribution, and precursor concentration can lead to inconsistent nucleation and growth, resulting in a broad size distribution and uneven silver shell thickness. Additionally, surface functionalization inefficiencies and nanoparticle aggregation during

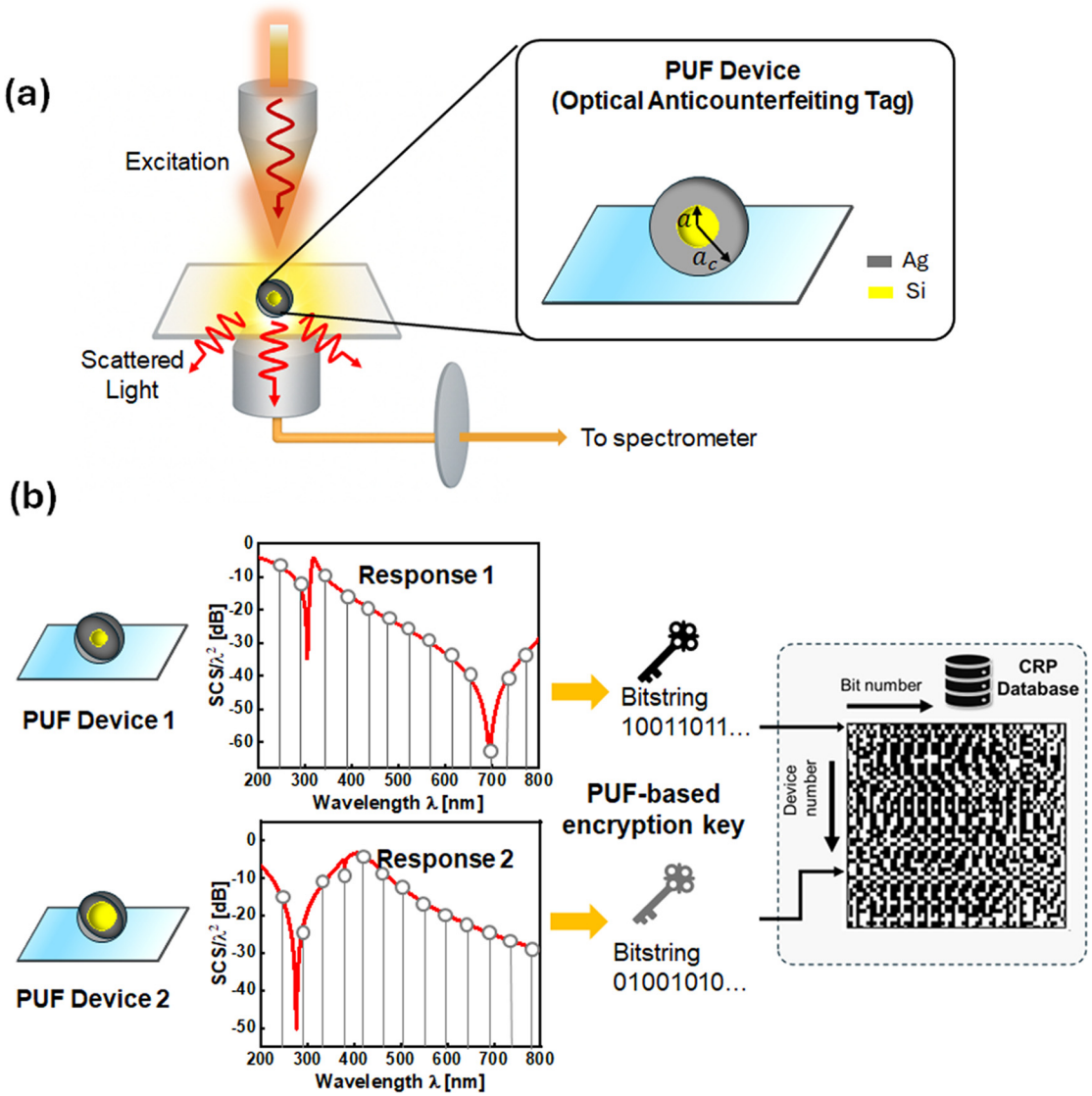


**FIG. 1.** (a) Schematics and (b) readout of the optical PUF label based on scattering responses of a core–shell nanoparticle exhibiting the Fano resonance; unique scattering responses measured by the scattering-type Scanning Near-field Optical Microscopy (s-SNOM) are digitized into binary PUF keys.

synthesis further contribute to randomness in material composition. In addition, the variation in ambient conditions and equipment calibration process can also introduce inconsistency among different batches despite the same synthesis process. According to the perturbation theorem, the drift/deformation of a resonant mode is sensitive to the local field intensity, which is inherently high at the Fano resonance with a high-quality factor (Q-factor). In other words, near the Fano resonance, even small geometric and/or material variations in the core–shell NP (e.g., unintentional and uncontrollable variations in nanomanufacturing processes) can result in remarkably different resonance line shape and linewidth. Consequently, random and ultrasensitive scattering responses can be exploited to produce optical PUF keys, as illustrated in Fig. 1. In the following, we will theoretically show that optical PUFs with high information capacity can be achieved with NP-based cryptographic random number generators (CRNGs). By digitally recognizing unique Fano-like resonant scattering responses of NPs, cryptographic keys with an encoding capacity of $2^{157}$ bits can be produced. Such a high encoding capacity is significantly greater than that of the traditional optical IDs or chipless RFIDs, whose encoding capacity is typically less than 32 bits. We will numerically and statistically demonstrate that the proposed PUF keys can exhibit high degree of uniqueness and irreproducibility, with high entropy in the binary bitmap composed of $10^3$ PUF instances (NPs with the stochastic fluctuations in their physical sizes and material profiles, following a normal distribution). Noticeably, the proposed nanoscale optical IDs are unobtrusive when compared with bar codes or QR, while their PUF keys stored in scattering responses are nearly impossible to be cloned and duplicate. The proposed PUF-based optical identification and anti-counterfeiting technique may pave the way toward the development of robust, secure, and tamper-resistant hardware encryption in the nano-photonic and nano-optical systems.

The core–shell nanoparticle-based PUF tags can be readily synthesized using various well-established methods, such as the top-down method based on the electron or UV lithography and laser-induced assembly[27] or the bottom-up method based on the chemical vapor deposition and seed-mediated growth method.[28–30] In the seed-mediated growth method (the most common approach to synthesize core–shell NP), the core NPs (i.e., seeds) are first functionalized with amine groups to facilitate plasmonic ion adsorption. Then, the reduction agent is introduced to reduce plasmonic ions onto the dielectric core surface, forming a uniform plasmonic shell.

Here, we consider a core–shell nanoparticle structure comprising a silicon nanosphere with relative permittivity $\varepsilon = 5$ and radius $a$, which is covered by a silver thin layer whose relative permittivity can be described by the Drude–Lorentz dispersion model: $\varepsilon_c = \varepsilon_\infty - f_p^2/[f(f + i\gamma)]$, where the plasma frequency $f_p = 2175$ THz and the damping rate fitted from the experimental data $\gamma = 4.35$ THz.[31] The SCS of this spherical nanostructure can be calculated using the Mie scattering theorem,[32,33] for which the TM and TE scattering coefficients of order $n$ for a non-magnetic nanoparticle ($\mu = 1$) are given as[15]

$$c_n^{TM} = -\frac{U_n^{TM}}{U_n^{TM} + iV_n^{TM}}, \tag{1a}$$

$$c_n^{TE} = -\frac{U_n^{TE}}{U_n^{TE} + iV_n^{TE}}. \tag{1b}$$

The total SCS is the sum of TM and TE scattering coefficients, given by

$$SCS = \frac{\lambda_0^2}{2\pi}\sum_{n=1}^{\infty}(2n+1)\left(|c_n^{TM}|^2 + |c_n^{TE}|^2\right), \tag{2}$$

where $\lambda_0$ is the free space wavelength. Since the core–shell NP is generally subwavelength, the dipolar scattering component ($n = 1$) dominates. Hence, under quasi-static approximation, the invisible mode ($U_1^{TM} = 0$) with low-scattering characteristics and the resonant scattering mode ($V_1^{TM} = 0$) with resonant scattering properties are, respectively, determined by the following equations:

$$\eta_c^2(\varepsilon - \varepsilon_c)(2\varepsilon_c + 1) + (\varepsilon + 2\varepsilon_c)(\varepsilon_c - 1) = 0, \tag{3a}$$

$$2\eta_c^2(\varepsilon - \varepsilon_c)(\varepsilon_c - 1) + (\varepsilon + 2\varepsilon_c)(\varepsilon_c + 1) = 0, \tag{3b}$$

where the filling ratio $\eta_c = a/a_c$. By adjusting the filling ratio and material properties of NPs, one can tailor the invisible mode with low scattering and the resonant scattering mode in the spectral range of interest. The coupling of these two modes resembles the Fano resonance line shape. Figure 2(a) presents the contour of the total SCS of core–shell NP as a function of the filling ratio and the wavelength of incident light, here $a_c = 50$ nm. The invisible and resonant scattering modes are highlighted with the blue and red lines, respectively. It can be seen from Fig. 2(a) that the core–shell NP exhibits a dual-band scattering suppression effect, accompanied by resonant scattering between two SCS minima. Figures 2(b)–2(d) present the evolution of spectral response of SCS (green lines) as the filling ratio varies from 0.25, 0.5 to 0.75. As can be seen in Fig. 2(c), two sharp resonant scattering modes can be obtained at 358 and 464 nm, while two invisible modes can be found at 285 and 413 nm. The exotic interaction between the bright and dark modes, with a sharp contrast in the total SCS, results in the peculiar dual Fano resonance. Unlike traditional Fano resonances arising from the interference between two different scattering orders, the dual Fano resonance observed here originates from the same scattering order.[34] It can be seen from Figs. 2(b) and 2(c) that decreasing (increasing) the filling ratio causes the adjacent resonant states (also applicable to the invisible states) to separate from each other, which results in sharpening (broadening) of Fano resonance linewidth. By properly tailoring resonances in the given spectral window, following the universally applicable guideline in Fig. 2(a), a conventional 2-bits optical ID tag can be built.[13] Such a concept is illustrated in Figs. 2(b)–2(d).

Next, we will study the manufacturing tolerance impact on the scattering responses of the core–shell NPs. In our statistical analysis and numerical experiment, the radii and relative permittivities of NPs are assumed to follow a Gaussian distribution:

$$P(x) = \frac{1}{\sqrt{2\pi}\sigma}e^{\frac{-(x-\mu)}{2\sigma^2}}, \tag{4}$$

where $\mu$ is the mean value of the NPs' design parameters and $\sigma$ is the standard deviation. In our statistical study, we assumed that the variation in radii of core and shell is normally distributed with a mean value of 37.5 and 50 nm and a standard deviation of 3.75 and 5 nm (10%). The permittivity of silver also follows a normal distribution in its Drude–Lorentz fit parameters,[31] of which the mean values of plasma frequency and the damping rate are $f_p = 2175$ THz and $\gamma = 4.35$ THz,

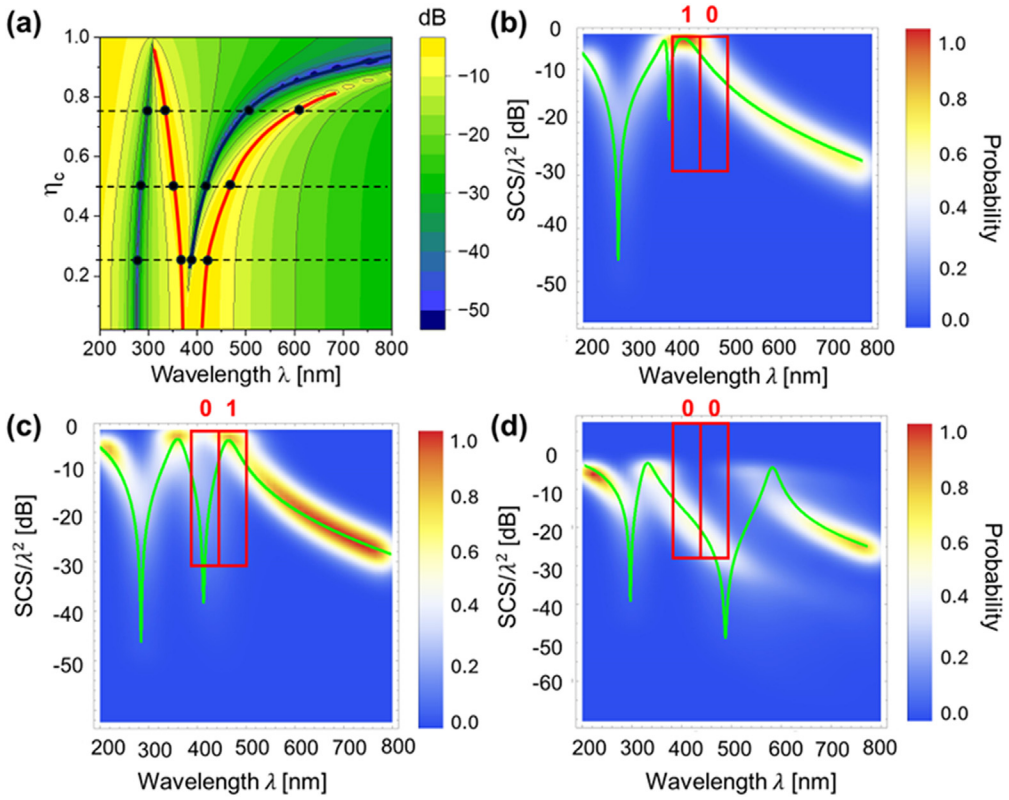


**FIG. 2.** (a) Contours of the normalized SCS of a core–shell (plasmonic-dielectric) NP as a function of wavelength and filling ratio. Traditional optical identification principle is illustrated in (b) and (c), for which a 2-digit tag is exemplified by a two-layered NP with different filling ratios; green lines: SCS of a core–shell NP with a filling ratio of (b) 0.25, (c) 0.5, and (d) 0.75; contours: probability of the normalized SCS for $10^3$ random core–shell NPs, whose radii and material properties follow a normal distribution.

respectively, and the standard deviation of plasma frequency ($\delta f_p$) and the damping rate ($\delta\gamma$) are 5% and 10%, respectively. Variations in these parameters follow a Gaussian distribution described in Eq. (4). Figures 2(b)–2(d) present the contours of probability of detection for the normalized SCS spectra for $10^3$ independent NPs with an error tolerance of 10% in their dimensions and material profiles ($a$= 37.5 nm, $a_c$= 50 nm, $f_p$ = 2175 THz, and $\gamma$ = 4.35 THz). In these colored contours, blue areas around the Fano resonance correspond to low probability of recurring event or high uncertainty, whereas red areas out of the Fano resonance band infer high detection probability. It is evident that near the Fano resonance, the probability of persistently observing the same resonant line shape is very low (i.e., high entropy). On the contrary, the scattering response out of the Fano resonance bands is rather insensitive to manufacturing imperfections, as can be seen in Figs. 2(b)–2(d), resulting in a high probability of duplication, thus lower entropy. Here, we find that even small variations in the physical size and material profiles of plasmonic core–shell NPs can lead to diversified SCS spectra due to the highly sensitive Fano resonance under perturbations. Such a high degree of uniqueness makes the scattering response each NPs an effective optical fingerprint for PUF-based identification, authentication, and nanoscale anti-counterfeiting applications.

Here, we exploit the normalized SCS spectra of plasmonic core–shell NPs with $\eta_c$ = 0.75 [Fig. 2(d)] to evaluate the PUF performance. The SCS spectra can be properly digitized to produce unique PUF-based encryption keys. Here, $10^3$ NPs (i.e., PUF instances) are randomly generated, with their SCS distributions shown in Fig. 2(d). In this optical PUF setup, the incident illumination and scattering response are regarded as the challenge and response. In the measurement setup, the Fano resonance in scattering characteristics can be measured by the scattering-type Scanning Near-field Optical Microscopy (s-SNOM), equipped with a custom-designed spectrometer system for SCS spectral analysis.[35] The scattered light is collected by the objective lens and sent to the spectrometer to collect the SCS response of core–shell NP, which is sketched in Fig. 1(a). The detected SCS spectra (within the Fano resonance band from 450 to 550 nm) are first normalized and then converted to a binary sequence. Here, each data point is converted to a 4-bit binary code, from 0000 to 1111, forming a 256-bit unique identifier (see the supplementary material for details of the analog-to-digital conversion).

Figures 3(a)–3(c) report bitmaps generated from $10^3$ Si NPs, $10^3$ Ag NPs, and $10^3$ core–shell Si/Ag NPs, respectively. For making a fair comparison, the dielectric and plasmonic NPs have the same mean diameter and material profiles as those of core–shell NPs. As seen in Figs. 3(a) and 3(b), binary bitmaps obtained from the scattering characteristics of dielectric or plasmonic NPs exhibit poor uniformity and low entropy. On the contrary, it is visible that the bitmap extracted from core–shell NPs is highly randomized, with equal distributions of

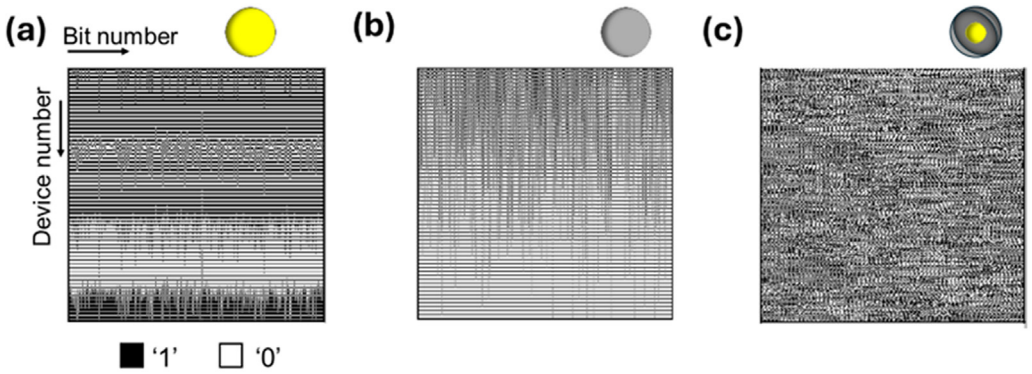


**FIG. 3.** Binary bitmap obtained from $10^3$ PUF instances made of (a) dielectric NPs, (b) plasmonic NPs, and (c) core–shell NPs.

0s and 1s throughout the bitmap [Fig. 3(c)]. In the following, we will fully characterize performance metrics of the proposed optical PUFs in terms of randomness, uniqueness, and encoding capacity.

We first evaluate the randomness of the PUF keys determined by the Shannon entropy $E_x$ and $E_y$ in the bitmaps,

$$E_x = -p_x \log_2 p_x - (1-p_x)\log_2(1-p_x), \tag{4a}$$

$$E_y = -p_y \log_2 p_y - (1-p_y)\log_2(1-p_y), \tag{4b}$$

where $p_x, p_y$ are the probability of obtaining "0" and "1" along the $x$ and $y$ axes of the bitmap, respectively. Ideally, $E_x$ and $E_y$ should be equal to unity, indicating a fully random entropy source with unbiased numbers of "0" and "1." Figures 4(a)–4(c) report $(E_x, E_y)$ of 256-bit PUF responses from $10^3$ dielectric NPs, $10^3$ plasmonic NPs, and $10^3$ Fano-resonant core–shell NPs, whose corresponding bitmaps are shown in Figs. 3(a)–3(c), respectively. The optical PUF keys generated from core–shell NPs show high cryptographic randomness and unpredictability [see Fig. 3(c)], with $(E_x, E_y) = (0.998, 0.995)$. The close-to-unity Shannon entropy can be attributed to the high entropy in the Fano resonance band. On the other hand, the Shannon entropy of PUF keys generated from dielectric and plasmonic NPs shows low cryptographic randomness [see Figs. 3(a) and 3(b)].

The National Institute of Standards and Technology (NIST) randomness test suite is commonly used for full assessment of randomness of binary sequeneces.[36] The NIST test suite consists of a set of tests, including frequency, block frequency, cumulative sums, runs, among others. Each test is considered as "pass" if the p-value is greater than 0.01. Table I presents the NIST randomness test results, showing that the PUF key generated from the core–shell NP passes all the NIST randomness tests, whereas the dielectric and plasmonic NPs failed in some of these tests.

The uniqueness of PUF keys is measured by the inter-device Hamming distance (inter-HD), which describes the number of non-identical bits when comparing two different PUF keys of the same bit length. Ideally, the inter-HD histogram fitted by a Gaussian distribution should be centered at 0.5 and have a zero-standard deviation, implying that the digitized keys of any two selected PUF instances are uncorrelated. The mean inter-HD is expressed as

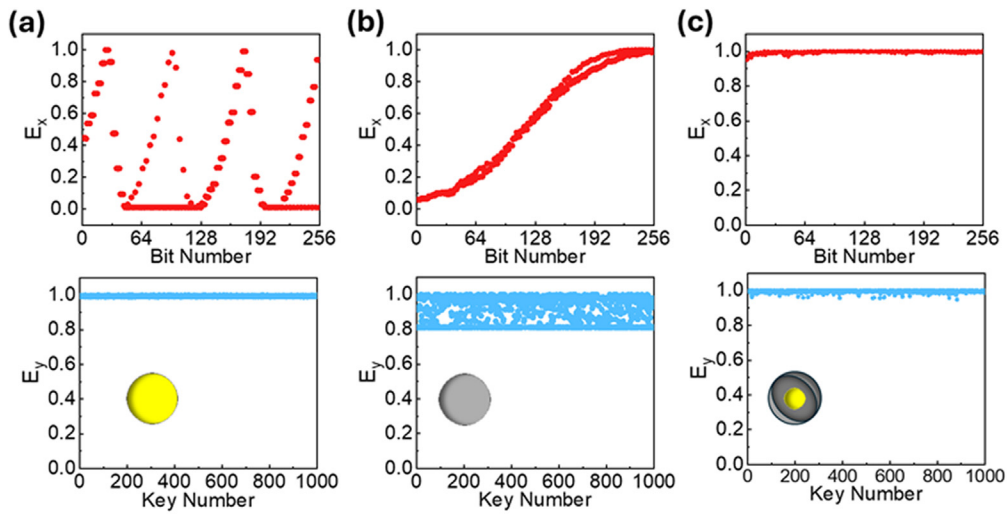


**FIG. 4.** Entropy (Ex, Ey) of (a) dielectric NP PUF instances, (b) plasmonic NP PUF instances, and (c) dielectric–plasmonic core–shell NP PUF instances.

**TABLE I.** P-values of PUF keys obtained from scattering characteristics of dielectric, plasmonic, and core–shell NPs.

| | Dielectric NP-based PUF | | Plasmonic NP-based PUF | | Core–shell NP-based PUF | |
|---|---|---|---|---|---|---|
| NIST randomness tests | P-values | Pass? | P-values | Pass? | P-values | Pass? |
| Frequency | 0.9622 | Yes | 0.8003 | Yes | 0.9779 | Yes |
| FB | 0.1710 | Yes | 0.0064 | No | 0.2607 | Yes |
| Runs | 0.2653 | Yes | 0.0661 | Yes | 0.4090 | Yes |
| LOR | 0.0077 | No | 0 | No | 0.0599 | Yes |
| FFT | 0.9900 | Yes | 0.9900 | Yes | 0.9813 | Yes |
| NOT (m = 5) | 0.9964 | Yes | 0.9967 | Yes | 0.9948 | Yes |
| Serial (m = 4) | 0.0194 | Yes | 0.0072 | No | 0.2625 | Yes |
| AppEn (m = 3) | 0 | No | 0 | No | 0.1646 | Yes |
| Cum.Sum. | 0.2317 | Yes | 0.0096 | No | 0.3060 | Yes |

$$\overline{HD}_{\text{inter}} = \frac{2}{N(N-1)} \sum_{i=1}^{N-1} \sum_{j=i+1}^{N} \frac{HD(K_i, K_j)}{L}, \tag{5}$$

where N is the number of PUF instances, L refers to bit length, and HD(Ki, Kj) is the inter-HD between i-th and j-th key. Figures 5(a)–5(c) show the inter-HD histogram of PUF keys generated from the dielectric, plasmonic, and core–shell NPs. The mean inter-HD ($\mu$) obtained from dielectric NP-based PUF and plasmonic NP-based PUF is 0.126 and 0.247, respectively, with corresponding standard deviations of 0.116 and 0.16. On the other hand, the core–shell NP-based PUF exhibits a sharp Gaussian distribution centered at $\mu = 0.501$, with standard deviation of $\sigma = 0.042$. Such values are close to the ideal values $(\mu, \sigma) = (0.5, 0)$, indicating that the proposed PUF keys generated from Fano-resonant NPs can have high uniqueness. Furthermore, the study of the PUF performance with respect to bit number is shown in Fig. 5(d). It can be seen that the mean value and the standard deviation of the inter-HD converge to the ideal values when the bit size is

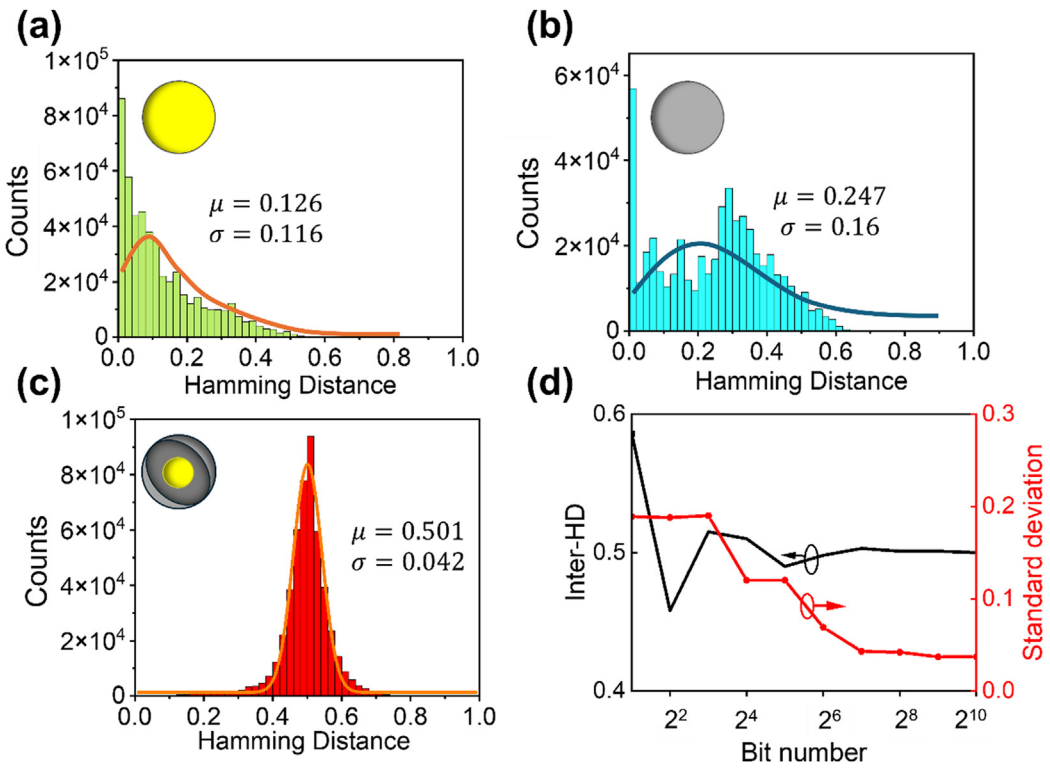


**FIG. 5.** Inter-Hamming distances (inter-HD) histogram obtained from PUF instances made of (a) dielectric NPs, (b) plasmonic NPs, (c) core–shell NPs, and (d) the mean and standard deviation of inter-HD obtained from PUF instances made of core–shell NPs as functions of the number of sample bits.

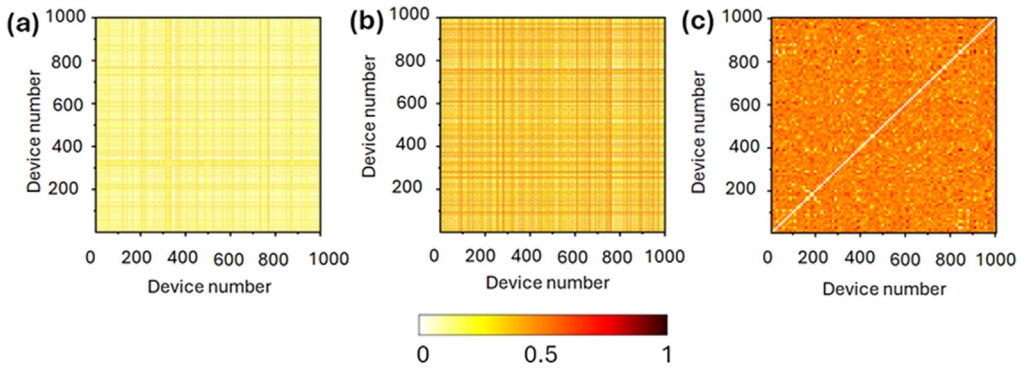


**FIG. 6.** Pairwise map among PUF instances made of (a) dielectric NPs, (b) plasmonic NPs, and (c) core–shell NPs.

greater than $2^6$. The uncorrelation between two distinct PUF instances can also be illustrated by the pairwise map of inter-HDs, of which the horizontal and vertical axes are the indices of PUF instances. The diagonal elements are set as 0 in accordance with no self-HD.

Figures 6(a)–6(c) show the pairwise inter-HD maps for PUF keys generated from dielectric NPs, plasmonic NPs, and core–shell NP PUF. The pairwise comparison maps in Figs. 6(a) and 6(b) show noticeable correlations between PUF keys. However, the pairwise comparison map in Fig. 6(c) shows a uniform distribution with a mean value of 0.5 in off diagonal elements, further validating that the proposed Fano resonance-enhanced PUF keys exhibit barely correlated in the bitmap. The encoding capacity of PUF responses is crucial for the optical tagging application. The coding capacity of PUF is defined as $c^k$, where $c$ is a number of bit states, here $c = 2$ for binary coding, and $k$ is the key size, which can be retrieved from the statistical results as Ref. 37. From the results in Fig. 5, the coding capacity of the optical ID tag-based Fano-resonant NP is $2^{157} = 1.827 \times 10^{47}$, which is considerably greater than that of the optical tag based on the non-resonant dielectric NPs PUF ($2^8 = 256$) or the plasmonic NP PUF ($2^7 = 128$). In sharp contrast, conventional optical ID tags shown in Figs. 2(c) and 2(d) have a low encoding capacity of only $2^2 = 4$.

Based upon the aforementioned statistical analysis and NIST test results, we can conclude that the proposed multilayered NP-based PUF devices with built-in Fano resonances can display unique electromagnetic fingerprints, such as scattering characteristics, for optical identification, tagging, and encryption applications.

In summary, we present here an approach to implement physical unclonable functions based on scattering characteristics of multilayered plasmonic-dielectric nanoparticles with built-in Fano resonances. Through our systematic numerical and statistical studies, we have demonstrated that the electromagnetic fingerprints in the Fano resonance window can be rather unique and irreplicable, showing excellent PUF performance benchmarks and, most importantly, a scalable encoding capacity. We envision that the proposed nanoparticle-based optical PUF instances will be beneficial for various optical identification, authentication, anti-counterfeiting, and cryptography applications.

See the supplementary material for a table about the detailed digital conversion from analog scattering cross section.

N.V. and P.-Y.C. would like to thank NSF (No. ECCS-2210977) for supporting this work. M.F. acknowledges support from King Abdullah University of Science and Technology.

## AUTHOR DECLARATIONS

### Conflict of Interest

The authors have no conflicts to disclose.

### Author Contributions

**Nga Vu:** Data curation (equal); Formal analysis (equal); Investigation (equal); Validation (equal); Writing – original draft (equal). **Mohamed Farhat:** Conceptualization (equal); Formal analysis (equal); Investigation (equal); Methodology (equal); Validation (equal); Writing – review & editing (equal). **Chien-Hao Liu:** Formal analysis (equal); Investigation (equal); Methodology (equal); Writing – review & editing (equal). **Pai-Yen Chen:** Conceptualization (equal); Formal analysis (equal); Funding acquisition (equal); Investigation (equal); Methodology (equal); Project administration (equal); Resources (equal); Software (equal); Supervision (equal); Writing – original draft (equal); Writing – review & editing (equal).

## DATA AVAILABILITY

The data that support the findings of this study are available from the corresponding author upon reasonable request.

## REFERENCES

[1]Y. Sonnefraud, N. Verellen, H. Sobhani, G. A. Vandenbosch, V. V. Moshchalkov, P. Van Dorpe, P. Nordlander, and S. A. Maier, "Experimental realization of subradiant, superradiant, and Fano resonances in ring/disk plasmonic nanocavities," ACS Nano **4**(3), 1664–1670 (2010).
[2]J. A. Fan, C. Wu, K. Bao, J. Bao, R. Bardhan, N. J. Halas, V. N. Manoharan, P. Nordlander, G. Shvets, and F. Capasso, "Self-assembled plasmonic nanoparticle clusters," Science **328**(5982), 1135–1138 (2010).
[3]N. Verellen, Y. Sonnefraud, H. Sobhani, F. Hao, V. V. Moshchalkov, P. V. Dorpe, P. Nordlander, and S. A. Maier, "Fano resonances in individual coherent plasmonic nanocavities," Nano Lett. **9**(4), 1663–1667 (2009).
[4]S. Zheng, Z. Ruan, S. Gao, Y. Long, S. Li, M. He, N. Zhou, J. Du, L. Shen, X. Cai, and J. Wang, "Compact tunable electromagnetically induced transparency and Fano resonance on silicon platform," Opt. Express **25**(21), 25655–25662 (2017).

[5]R. Ortuño, M. Cortijo, and A. Martínez, "Fano resonances and electromagnetically induced transparency in silicon waveguides loaded with plasmonic nanoresonators," J. Opt. **19**(2), 025003 (2017).
[6]A. A. Bogdanov, K. L. Koshelev, P. V. Kapitanova, M. V. Rybin, S. A. Gladyshev, Z. F. Sadrieva, K. B. Samusev, Y. S. Kivshar, and M. F. Limonov, "Bound states in the continuum and Fano resonances in the strong mode coupling regime," Adv. Photonics **1**, 016001 (2019).
[7]C. Zhou, X. Qu, S. Xiao, and M. Fan, "Imaging through a fano-resonant dielectric metasurface governed by quasi—bound states in the continuum," Phys. Rev. Appl. **14**(4), 044009 (2020).
[8]B. Luk'yanchuk, N. I. Zheludev, S. A. Maier, N. J. Halas, P. Nordlander, H. Giessen, and C. T. Chong, "The Fano resonance in plasmonic nanostructures and metamaterials," Nat. Mater. **9**(9), 707–715 (2010).
[9]R. Zektzer, M. T. Hummon, L. Stern, Y. Sebbag, Y. Barash, N. Mazurski, J. Kitching, and U. Levy, "A chip-scale optical frequency reference for the telecommunication band based on acetylene," Laser Photon Rev. **14**(6), 1900414 (2020).
[10]W. Zhao, X. Leng, and Y. Jiang, "Fano resonance in all-dielectric binary nanodisk array realizing optical filter with efficient linewidth tuning," Opt. Express **23**(5), 6858–6866 (2015).
[11]G. Cao, S. Dong, L.-M. Zhou, Q. Zhang, Y. Deng, C. Wang, H. Zhang, Y. Chen, C.-W. Qiu, and X. Liu, "Fano resonance in artificial photonic molecules," Adv. Opt. Mater. **8**(10), 1902153 (2020).
[12]K. P. Heeg, C. Ott, D. Schumacher, H.-C. Wille, R. Röhlsberger, T. Pfeifer, and J. Evers, "Interferometric phase detection at X-ray energies via Fano resonance control," Phys. Rev. Lett. **114**(20), 207401 (2015).
[13]F. Monticone, C. Argyropoulos, and A. Alù, "Multilayered plasmonic covers for comblike scattering response and optical tagging," Phys. Rev. Lett. **110**(11), 113901 (2013).
[14]A. Alù and N. Engheta, "Achieving transparency with plasmonic and metamaterial coatings," Phys. Rev. E **72**(1), 016623 (2005).
[15]C. Argyropoulos, P.-Y. Chen, F. Monticone, G. D'Aguanno, and A. Alù, "Nonlinear plasmonic cloaks to realize giant all-optical scattering switching," Phys. Rev. Lett. **108**(26), 263905 (2012).
[16]E. Prodan, C. Radloff, N. J. Halas, and P. Nordlander, "A hybridization model for the plasmon response of complex nanostructures," Science **302**(5644), 419–422 (2003).
[17]R. Rezaiesarlak and M. Manteghi, "Complex-natural-resonance-based design of chipless RFID tag for high-density data," IEEE Trans. Antennas Propag. **62**(2), 898–904 (2014).
[18]B. Wang, P. Yu, W. Wang, X. Zhang, H. C. Kuo, H. Xu, and Z. M. Wang, "High-Q plasmonic resonances: Fundamentals and applications," Adv. Opt. Mater. **9**(7), 2001520 (2021).
[19]A. Chaudhuri, K. Mandaviya, P. Badelia, and S. Ghosh, "Optical character recognition systems for Hindi language," in *Optical Character Recognition Systems for Different Languages with Soft Computing* (Springer, Cham, 2017), Vol. 352, pp. 193–216.
[20]B. L. Volodin, B. Kippelen, K. Meerholz, B. Javidi, and N. Peyghambarian, "A polymeric optical pattern-recognition system for security verification," Nature **383**(6595), 58–60 (1996).
[21]X. Wang, W. Chen, and X. Chen, "Optical information authentication using compressed double-random-phase-encoded images and quick-response codes," Opt. Express **23**(5), 6239–6253 (2015).
[22]R. Fu, K. Chen, Z. Li, S. Yu, and G. Zheng, "Metasurface-based nanoprinting: Principle, design and advances," Opto-Electron. Sci. **1**(10), 220011 (2022).
[23]S. S. Mousavi Khaleghi, D. Wen, J. Cadusch, and K. B. Crozier, "High resolution multicolor holograms encoded into color print images with hybrid dielectric/plasmonic metasurfaces," Appl. Phys. Lett. **126**(5), 051102 (2025).
[24]C. Xu, C. Huang, D. Yang, L. Luo, and S. Huang, "Photo-luminescent photonic crystals for anti-counterfeiting," ACS Omega **7**(8), 7320–7326 (2022).
[25]J. B. Lassiter, H. Sobhani, J. A. Fan, J. Kundu, F. Capasso, P. Nordlander, and N. J. Halas, "Fano resonances in plasmonic nanoclusters: Geometrical and chemical tunability," Nano Lett. **10**(8), 3184–3189 (2010).
[26]S. Zhu, D. Deng, M. T. Nguyen, Y. T. R. Chau, C. Y. Wen, and T. Yonezawa, "Synthesis of Au@ $Cu_2O$ core–shell nanoparticles with tunable shell thickness and their degradation mechanism in aqueous solutions," Langmuir **36**(13), 3386–3392 (2020).
[27]S. Kumari, S. Raturi, S. Kulshrestha, K. Chauhan, S. Dhingra, K. András, K. Thu, R. Khargotra, and T. Singh, "A comprehensive review on various techniques used for synthesizing nanoparticles," J. Mater. Res. Technol. **27**, 1739–1763 (2023).
[28]M. B. Gawande, A. Goswami, T. Asefa, H. Guo, A. V. Biradar, D. L. Peng, R. Zboril, and R. S. Varma, "Core–shell nanoparticles: Synthesis and applications in catalysis and electrocatalysis," Chem. Soc. Rev. **44**(21), 7540–7590 (2015).
[29]K. Mallik, M. Mandal, N. Pradhan, and T. Pal, "Seed mediated formation of bimetallic nanoparticles by UV irradiation: A photochemical approach for the preparation of "core−shell" type structures," Nano Lett. **1**(6), 319–322 (2001).
[30]C. C. Huang, Z. Yang, and H. T. Chang, "Synthesis of dumbbell-shaped Au−Ag core−shell nanorods by seed-mediated growth under alkaline conditions," Langmuir **20**(15), 6089–6092 (2004).
[31]P. B. Johnson and R. W. Christy, "Optical constants of the noble metals," Phys. Rev. B **6**(12), 4370–4379 (1972).
[32]F. Monticone, C. Argyropoulos, and A. Alù, "Layered plasmonic cloaks to tailor the optical scattering at the nanoscale," Sci. Rep. **2**(1), 912 (2012).
[33]A. Alù and N. Engheta, "Polarizabilities and effective parameters for collections of spherical nanoparticles formed by pairs of concentric double-negative, single-negative, and / or double-positive metamaterial layers," J. Appl. Phys. **97**(9), 094310 (2005).
[34]S. Kay, *Intuitive Probability and Random Processes Using MATLAB®* (Springer Science & Business Media, 2006).
[35]P. Fan, Z. Yu, S. Fan, and M. L. Brongersma, "Optical Fano resonance of an individual semiconductor nanostructure," Nat. Mater. **13**(5), 471–475 (2014).
[36]A. Rukhin, J. Soto, J. Nechvatal, M. Smid, E. Barker, S. Leigh, M. Levenson, M. Vangel, D. Banks, A. Heckert, and J. Dray, *A Statistical Test Suite for Random and Pseudorandom Number Generators for Cryptographic Applications* (US Department of Commerce, Technology Administration, National Institute of Standards and Technology, Gaithersburg, MD, 2001), Vol. 22, p. 1.
[37]Z. Hu, J. M. M. L. Comeras, H. Park, J. Tang, A. Afzali, G. S. Tulevski, J. B. Hannon, M. Liehr, and S. J. Han, "Physically unclonable cryptographic primitives using self-assembled carbon nanotubes," Nat. Nanotechnol. **11**(6), 559–565 (2016).